Electronic Supporting Information

The 3D $[(Cu_2Br_2)\{\mu\text{-}EtS(CH_2)_4SEt\}]_n$ Material: A Rare Example of a Coordination Polymer Exhibiting Triplet-Triplet Annihilation

Antoine Bonnot, Paul-Ludovic Karsenti, Frank Juvenal, Christopher Golz, Carsten Strohmann, Daniel Fortin, Michael Knorr, and Pierre D. Harvey

Table of Content

Experimental Section page

Experimental Section

Material:

CuI, CuBr, CuCl, EtCN and MeCN were purchased from Sigma-Aldrich or Acros. 1,4-bis(ethylsulfanyl)butane **L1** was prepared in similar manner as described in the literature by treatment of an ethanolic solution of *in situ* generated KSEt with 0.5 equivalents of 1,4-dibromobutane. [1]

Preparation of **CP1** was prepared according a modification of a literature procedure by treatment of CuI (385 mg, 2.0 mmol) with **L1** (178 mg, 1.0 mmol) in MeCN. Replacement of MeCN by EtCN provided better quality crystals and gave the material in higher yield (76 %) compared to the literature protocol.

Preparation of **CP2.** In a Schlenk tube, CuBr (286 mg, 2.0 mmol) was dissolved in degassed MeCN (10 mL) and $EtS(CH_2)_4SEt$ (374 mg, 2.1 mmol) was added. After stirring for 1h, the slight greenish solution was stored for 1d in a refrigerator a 5° C. Yellow brownish blocks of **CP2** were formed progressively and separated after 2 d. Yield (73 %). Anal. Calcd. for $C_8H_{18}Br_2Cu_2S_2$ (465.26): C, 20.02; H, 6.35; S, 13.78. Found: C, 19.82; H, 6.26; S, 13.90

---

[1] E. Anklam, Synthesis., 1987, 9, 841.

Powder XRD measurements: **CP1** and **CP2** were mixed with a small amount of paratone oil, cut to approximately 0.3 X 0.3 X 0.3 mm^3, and place on a sample holder mounted at 173.2 K on a Bruker APEX DUO X-Ray diffractometer. 6 correlated runs per sample with Phi Scan of 360 degrees and exposure times of 270 seconds were collected with the Cu micro-focus anode (1.54184 Å) and the CCD APEX II detector at 150 mm distance. These runs, from -12 to -72°2θ and 6 to 36°ω, were then treated and integrated with the XRW2 Eval Bruker software to produce WAXD diffraction patterns from 2.5 to 82°2θ. The patterns were treated with Diffrac.Eva version 2.0 from Bruker.

Single crystal XRD measurement: A colorless single crystal of **CP1** was mounted on a Nonius Kappa Apex-II CCD diffractometer equipped with a nitrogen jet stream low-temperature system (Oxford Cryosystems). The X-ray source was graphite-monochromated Mo-K_α radiation (λ = 0.71073 Å) from a sealed tube. Data collections have been carried out at five different temperatures – 115, 155, 195, 235 and 275 K on one crystal. The lattice parameters were obtained by least-squares fit to the optimized setting angles of the entire set of collected reflections. Intensity data were recorded as ϕ and ω scans with κ offsets. No significant intensity decay or temperature drift was observed during data collections. Data were reduced by using DENZO software without applying absorption corrections; the missing absorption corrections were partially compensated by the data scaling procedure in the data reduction. The structure was solved by direct methods with SIR92 program of Altomare et al. Refinements were carried out by full-matrix least-squares on F^2 using SHELXL-97 program on the complete set of reflections.[2] All non–hydrogen atoms were refined with anisotropic thermal parameters, whereas the H atoms were treated in a riding mode.

Crystals of **CP2** were mounted on a Bruker APEX diffractometer (D8 three-circle goniometer) (Bruker AXS). Data collection, cell determination and refinement: Smart version 5.622 (Bruker AXS, 2001); integration: SaintPlus version 6.02 (Bruker AXS, 1999); empirical absorption correction: Sadabs version 2.01 (Bruker AXS, 1999). The crystals were mounted at room temperature but the crystal structure determination was performed at -100 ◦C (type of radiation: Mo-Kα, λ = 0.71073 Å). The structures were solved applying direct and Fourier methods, using SHELXS-90 and SHELXL-97.[ref] All non–hydrogen atoms were refined with anisotropic thermal parameters, whereas the H atoms were treated in a riding mode.

Instrumentation: The solid-state UV−vis spectra were recorded on a Varian Cary 300 Bio UV-Vis spectrophotometer at 298 and 77 K. The solid-state emission, excitation and chromaticity diagrams were measured on a phosphorimeter QuantaMaster 400 from Photon Technology International (PTI). The-ns emission lifetime measurements were performed with the FLS980 phosphorimeter using a 378 nm picosecond pulsed diode

---

[2] G. M. Sheldrick, Acta Cryst., 2008, **A64**, 112.

laser (fwhm = 90 ps) as an excitation source. Data collection on the FLS980 system was performed using a time correlated single photon counting (TCSPC) system. The μs-emission lifetimes were measured on a spectrofluorometer model FSP920 from Edinburg Instrument using a Xe flash lamp (fwhm 2 μs). The solid state emission quantum yield was measured on Horiba Fluorolog III equipped of an integration sphere. The TGA traces were acquired on a Setsy's 24 apparatus from Setaram, in the 25 and 900 °C range at scanning rate of 5°/min under a N_2 atmosphere. Gas sorption isotherms at low-pressure ranging between 0 to 1100 mbar (~1.1 atm) were measured using Micrometrics instrument 'Accelerated Surface Area and Porosimetry' (ASAP 2020) analyzer (i.e. BET). For the isotherms, warm and cold free space correction measurements were performed using ultra-high purity He gas with 99.999% of purity. The gas used was of high grade with purity of 99.999%. The measurements were performed at 77K.

Fast kinetic emission decay measurements: The laser source was the SHG of a Soltice (Spectra Physics) Ti-Sapphire laser (λ_{exc} = 398 nm; FWHM = 75-100 ps; pulse energy = 0.1 μJ/pulse, rep. rate = 1 kHz; spot size ~ 500 μm). The IRF became of a HWHM of 8 ps after passing through the optics. The detector was a Streak Camera (Axis-TRS, Axis Photonique Inc.) with typically less than 8 ps resolution. The results were also globally analysed with the program Glotaran (http://glotaran.org) permitting to extract a sum of independent exponentials ($I(\lambda, t) = C_1(\lambda) \bullet \exp(-t/\tau_1) + C_2(\lambda) \bullet \exp(-t/\tau_2) + \ldots$).

Computations: All density functional theory (DFT) and time dependent density functional theory (TD-DFT) calculations were performed with Gaussian 09[3] at the Université de Sherbrooke with the Mammouth supercomputer supported by *Le Réseau Québécois De CalculsHautes Performances*. .cif file from DRX structures has been used like optimized structure for calculations. The DFT (singlet and triplet energy states) as well as TD-DFT calculations were carried out using the B3LYP method. VDZ (valence double ζ) with SBKJC effectivecore potentials were used for all Cu and Br atoms and 3-21g* basis set was used for C, H and S atoms.[4] The calculated absorption spectra were obtained from GaussSum 2.1. [5]

---

[3] (a) M. J. Frisch, et al. *Gaussian, Inc., Wallingford CT*, 2004; (b) P. Hohenberg, and W. Kohn. *Phys. Rev*., 1964, **136**, B864; (c) P. Hohenberg, and W. Kohn. *J. Phys. Rev*., 1965, **140**, A1133; (d) R. G. Parr, and W. Yang. *Density-functional theory of atoms and molecules*, Oxford Univ. Press, Oxford, 1989; (e) D. R. Salahub, and M. C. Zerner. *The Challenge of d and f Electrons*, Amer. Chem. Soc., Washington, D.C., 1989; R. Bauernschmitt, and R. Ahlrichs. *Chem. Phys. Lett*. 1996, **256**, 454; (f) M. E. Casida, C. Jamorski, K. C. Casida, and D. R. Salahub. *J. Chem. Phys.,* 1998, **108**, 4439; (g) R. E. Stratmann, G. E. Scuseria, and M. J. Frisch. *J. Chem. Phys.,* 1998, **109**, 8218; (h) C. Lee, W. Yang, and R. G. Parr. *Phys. Rev. B*, 1988, 37, 785

[4] (a). Binkley JS, Pople JA and Hehre WJ. *J. Am. Chem. Soc.* 1980; **102**: 939; (b). Gordon MS, Binkley JS, Pople JA, Pietro WJ and Hehre WJ. *J. Am. Chem. Soc.* 1982; **104**: 2797; (c) Pietro WJ, Francl MM, Hehre WJ, Defrees DJ, Pople JA andBinkley JS. *J. Am. Chem. Soc.* 1982; **104**: 5039; (d) Dobbs KD and Hehre WJ. *J. Comput. Chem.* 1986; **7**: 359; (e) Dobbs KD and Hehre

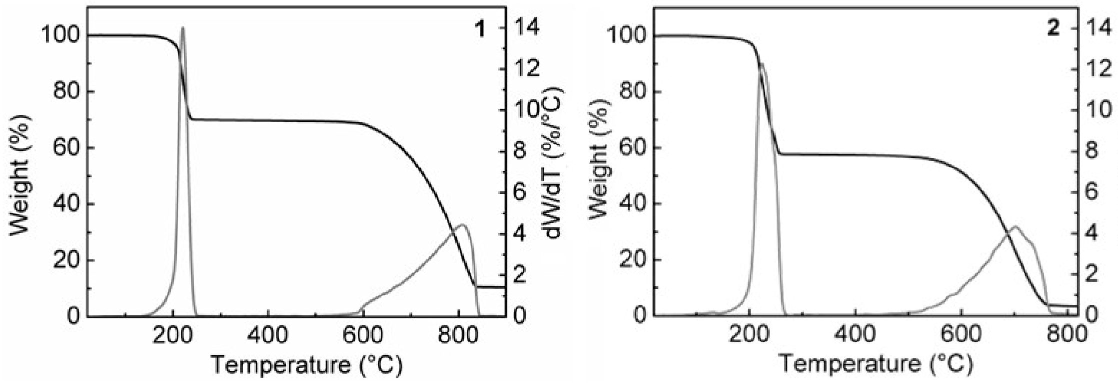

Figure S1. TGA (black) and first derivative (grey) TGA traces of **CP1** (left) and **CP2** (right) recorded under nitrogen atmosphere.

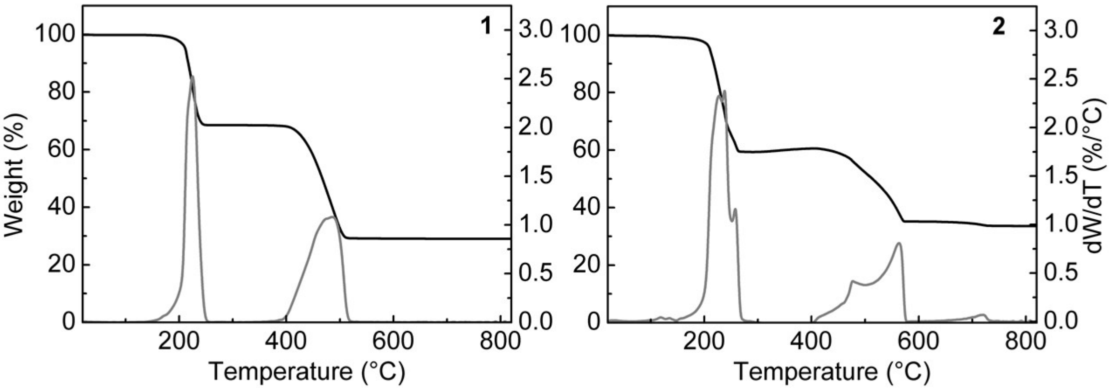

Figure S2. TGA (black) and first derivative (grey) TGA traces of **CP1** (left) and **CP2** (right) recorded under oxygenated atmosphere.

WJ. *J. Comput. Chem.* 1987; **8**: 861. (f) Dobbs KD and Hehre WJ. *J. Comput. Chem.* 1987; **8**: 880

[5] O'Boyle NM, Tenderholt AL and Langner KM. *J. Comp. Chem.* 2008; **29**: 839

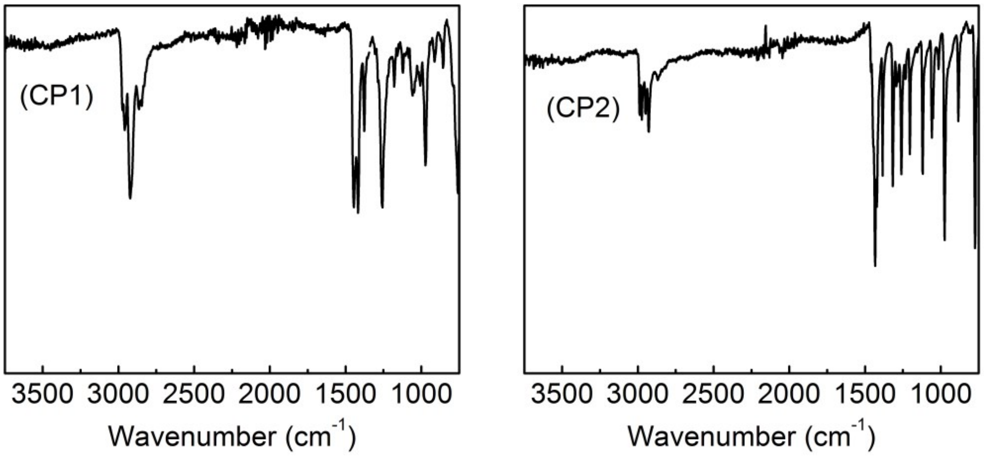

Figure S3. IR spectra of **CP 1** and **CP2** stressing the absence of water and CN function.

Table S1. Crystal data, data collection and structure refinement for **CP1** and **CP2**.

	CP1(100 K)	**CP2** (293 K)	**CP2** (123 K)
Formula	$C_8H_{18}Cu_2I_2S_2$	C_4H_9BrCuS	C_4H_9BrCuS
Formula weight	559.22	232.62	232.62
Temperature/K	104	293(2)	123(2)
Wavelength/Å	0.71073	1.54186 Å	0.71073
Crystal system	tetragonal	monoclinic	monoclinic
Space group	$P4_3$	P 1 21/n 1	P 21/n
a/Å	11.8564(11)	9.0604(9)	9.0497(5)
b/Å	11.8564(11)	6.9028(7)	6.8756(4)
c/Å	21.415(2)	11.0330(10)	10.9978(6)
β /°	90	108.698(4)	108.886(2)
Volume/ $Å^3$	3010.4(6)	653.61(11)	646.59(6)
Z	8	4	1
Density (calculated) g/cm^3	2.68	2.364	2.390
Absorption coefficient/mm^{-1}	7.122	13.834	9.752
F(000)	2096	452	452
Crystal size/mm	0.026 x 0.170 x 0.01	0.020 x 0.100 x 0.330	0.174 x 0.092 x 0.035
Theta range for data collection/°	5.218 to 55.996	5.52 to 71.14	7.072 to 55.986
Index ranges	-15<=h<=15, -15<=k<=15, -28<=l<=28	-11<=h<=10, -8<=k<=8, -10<=l<=13	-11<=h<=11, -9<=k<=8, -14<=l<=14
Reflections collected	135148	6122	17487
Independent reflections	7273 [R(int) = 0.0440	1180 [R(int) = 0.0625]	1545 [R(int) = 0.0401
Refinement method	Full-matrix least-squares on F^2	Full-matrix least-squares on F^2	Full-matrix least-squares on F^2
Data / restraints / parameters	7273 / 1 / 298	1180 / 0 / 66	1545 / 0 / 66
Goodness-of-fit on F^2	1.093	1.068	1.076
Final *R* indices [*I*>2sigma(I)]	R1 = 0.0231, wR2 = 0.0528	R1 = 0.0707, wR2 = 0.2152	R1 = 0.0145, wR2 = 0.0333
R indices (all data)	R1 = 0.0244, wR2 = 0.0533	R1 = 0.0796, wR2 = 0.2358	R1 = 0.0160, wR2 = 0.0337
Larg. diff. peak and hole/e.$Å^{-3}$	0.92 and -076 $eÅ^{-3}$	1.369 and -1.012 $eÅ^{-3}$	0.36 and -0.035 $eÅ^{-3}$

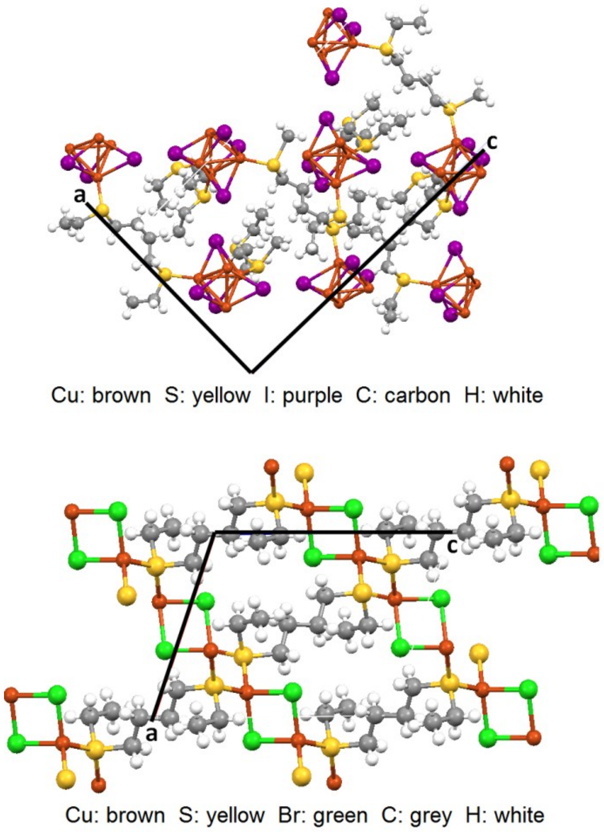

Figure S4. View of the Packing for **CP1** and **CP2** at the b axes along.

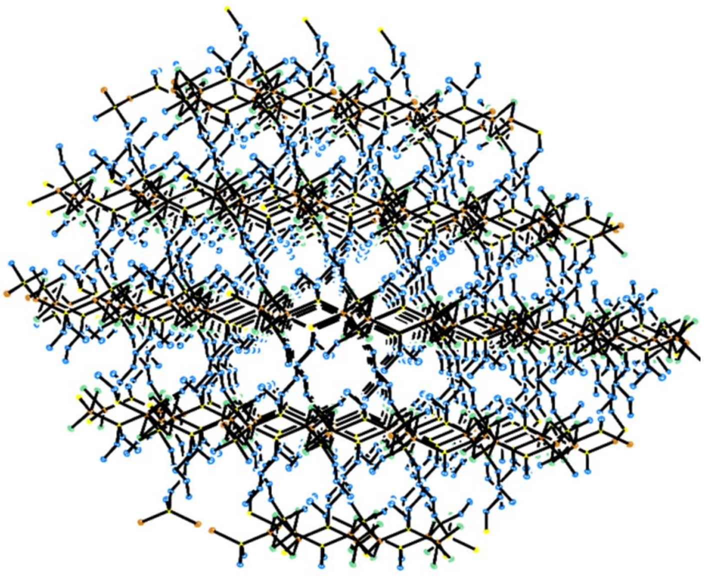

Figure S5. 3D representation of **CP2** network generated using Ortep as image generator.

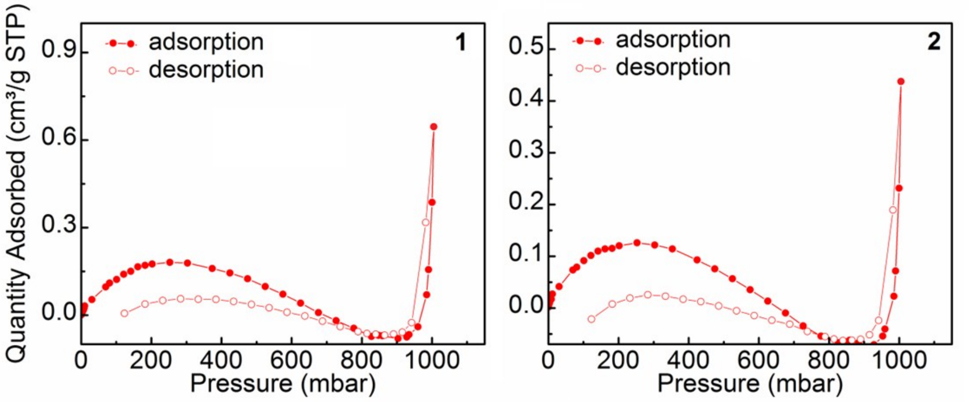

Figure S6. N_2 sorption isotherm of **CP1** (left) and **CP2** (right) measured at 77K. Closed circles: adsorption and open circles: desorption.

Table S2. Selected distances form the crystal data of **CP1** and **CP2** at 173 K.

CPs	**CP1**	**CP2**
SBU	$Cu_4(\mu_3\text{-}I)_4$	$Cu_2(\mu_3\text{-}Br)_2$
$d_{Cu..Cu}$ (A)	2.660 (1)	3.456 (2)
d_{2L} (A)	<5	-^{a}
d_{2C} (A)	9.34328^{b}	4.23689 ^{b}
	15.03952^{c}	6.87420 ^{c}
	8.709^{c}	8.66595 ^{c}

[a] 3D polymers, do not exhibit separations between two consecutive layers
[b] 2 clusters connected together by the same ligand,
[c] 2 clusters closed through the void (not directly connected)

Table S3. Cu–Cu, Cu–S and Cu–Br distances (Å) for **CP2** at different temperatures.

Atom bounds	Distances at 298 K	Distances at 173K
Cu1–Br1	2.543(2)	2.536(2)
Cu1–Br2	2.474(2)	2.473(2)
Cu1– Cu2	3.459(2)	3.456(2)
Br1–Br2	3.635(2)	3.627(2)
Cu1–S1	2.368(3)	2.352(3)
Cu2–S2	2.328(3)	2.313(3)
Two closest rhomboids	4.264(2)	4.237(2)

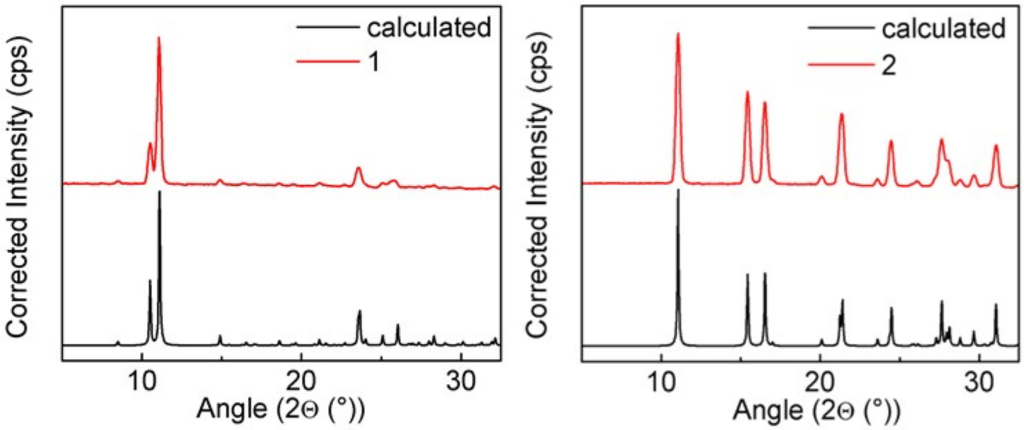

Figure S7. Experimental powder XRD patterns (red) of **CP1** (left) and **CP2** (right) compared to the calculated ones (black) using the single crystal X-ray data.

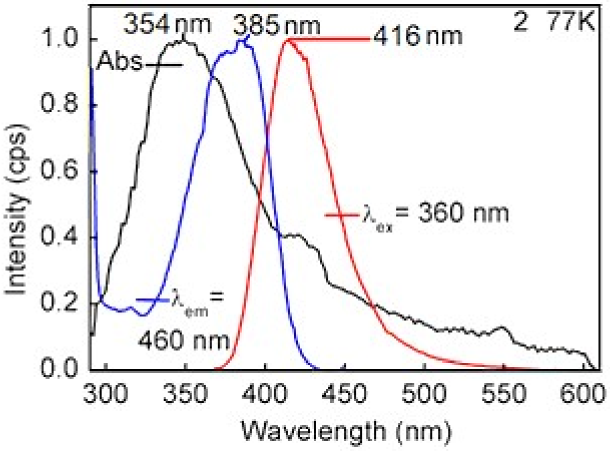

Figure S8. Solid-state absorption (black), excitation (blue) and emission spectra (red) of **CP2** at 77 K.

Table S4. Calculated electronic transition energy, oscillator strength (f) and major contributions of the first 50 singlet-singlet electronic transitions for **CP2**.

λ (nm)	f	Major contributions (%)
285.4	0.0004	H-4→L+2 (16), H-4→L+4 (16)
285.4	0.0006	H-5→L+2 (18), H-5→L+4 (17)
282.3	0.0011	H-1→L+6 (19)
282.3	0.0069	HOMO→L+7 (23)
281.3	0.0014	H-3→L+10 (15)
281.3	0.0014	H-2→L+10 (14)
279.7	0.0037	H-16→LUMO (14), H-12→LUMO (17), H-8→LUMO (23)
278.2	0.0043	H-17→L+1 (14), H-13→L+1 (16), H-9→L+1 (22)
277.7	0.0197	H-20→LUMO (27)
276.8	0.081	H-3→L+3 (6), H-3→L+4 (4), H-3→L+6 (5)
276.7	0.0006	H-9→L+6 (3), H-5→L+3 (2), H-5→L+6 (3)
276.0	0.0132	H-21→L+1 (23)
274.8	0.0048	H-4→L+5 (10)
274.6	0.0018	H-5→L+5 (10)
273.3	0.001	H-11→L+2 (15), H-10→L+4 (13)
273.3	0.0178	H-11→L+4 (16), H-10→L+2 (12)
272.5	0.0115	H-8→L+5 (5), H-8→L+6 (3), H-8→L+7 (4)
272.5	0.0114	H-13→L+6 (3), H-9→L+2 (4), H-9→L+5 (5)
271.9	0.0138	HOMO→L+6 (15)
271.8	0.0212	H-1→L+7 (14)
271.2	0.0203	H-24→LUMO (5), H-16→LUMO (4), H-5→L+12 (2)
271.2	0.0139	H-24→LUMO (14)
271.1	0.0017	H-5→L+3 (4), H-5→L+4 (7), H-5→L+11 (8)
270.0	0.0359	H-7→L+8 (10)
269.9	0.0152	H-25→L+1 (4), H-17→L+1 (3), H-10→L+5 (5)
269.8	0.008	H-6→L+7 (10), H-6→L+8 (10)
269.7	0.0096	H-25→L+1 (14)
269.2	0	H-15→L+2 (4), H-15→L+5 (4), H-11→L+2 (5)
268.2	0.0243	H-12→L+2 (6), H-12→L+5 (6), H-12→L+6 (3)
268.0	0.0118	H-13→L+2 (5), H-13→L+5 (5), H-13→L+6 (5)
267.6	0.0163	H-6→L+15 (13)
267.4	0.015	H-9→L+2 (3), H-9→L+5 (4), H-7→L+6 (3)
267.2	0.0103	H-8→L+10 (3), H-6→L+6 (2), H-6→L+15 (5)
267.1	0.0129	H-9→L+10 (4), H-7→L+14 (4), H-7→L+15 (4)
266.8	0.0087	H-13→L+10 (2), H-9→LUMO (3), H-9→L+10 (2)
266.8	0.0035	H-12→L+10 (2), H-8→L+1 (3), H-8→L+10 (3)
266.7	0.0019	HOMO→LUMO (29)
266.3	0.0039	H-7→L+1 (4), H-7→L+8 (6), H-7→L+13 (2)
265.8	0.0157	H-1→L+3 (13)

265.7	0.019	H-6→L+7 (4), H-6→L+9 (7), H-6→L+15 (5)
265.2	0.0013	HOMO→LUMO (41)
264.7	0.0007	H-1→L+1 (52)
264.5	0.0014	H-9→L+3 (3), H-9→L+4 (3), H-9→L+7 (2)
264.4	0.0957	H-15→L+4 (3), H-5→L+3 (8)), H-4→L+3 (8)
264.4	0.0006	H-9→L+3 (4), H-5→L+3 (7), H-4→L+3 (6)
264.2	0.0088	H-1→L+1 (10), H-1→L+14 (10)
264.2	0.0012	HOMO→L+15 (11), HOMO→L+16 (11)
264.1	0.0773	H-9→L+3 (5), H-9→L+7 (4), H-8→L+3 (4)
263.1	0.0351	H-16→L+2 (5), H-16→L+5 (7), H-16→L+6 (3)
263.0	0.0333	H-17→L+5 (3), H-15→L+4 (3), H-14→L+5 (8)

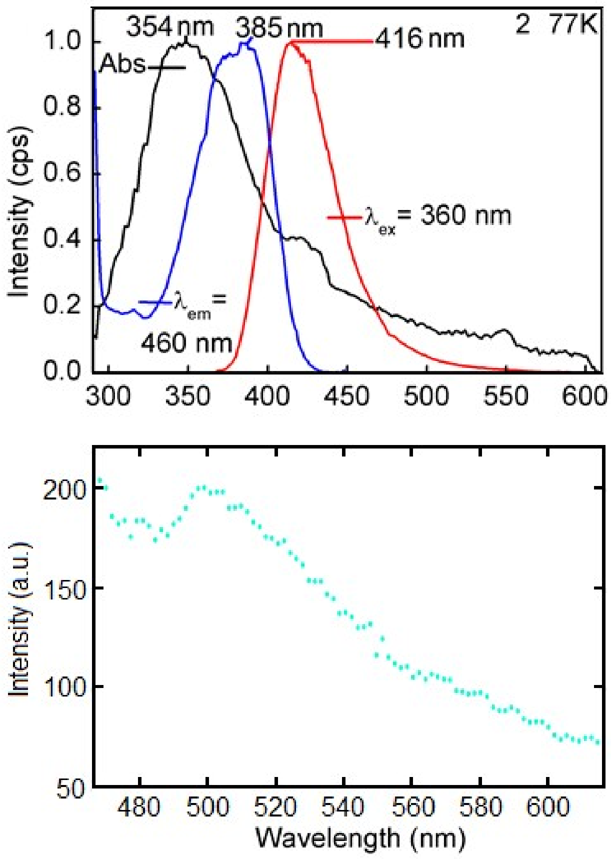

Figure S9. Top: solid-state absorption (black), excitation (blue) and emission spectra (red) of **CP2** at 77 K. The bumps near 550 nm and the large slope in baseline between 400 and 600 nm, are instrumental artefacts. Bottom, emission spectrum of **CP2** at 77 K using a pulse power of 0.9 μJ/pulse at 1 KHz, λ_{exc} = 397 nm, and pulse width ~ 0.1 ps (spot size ~ 1 mm).

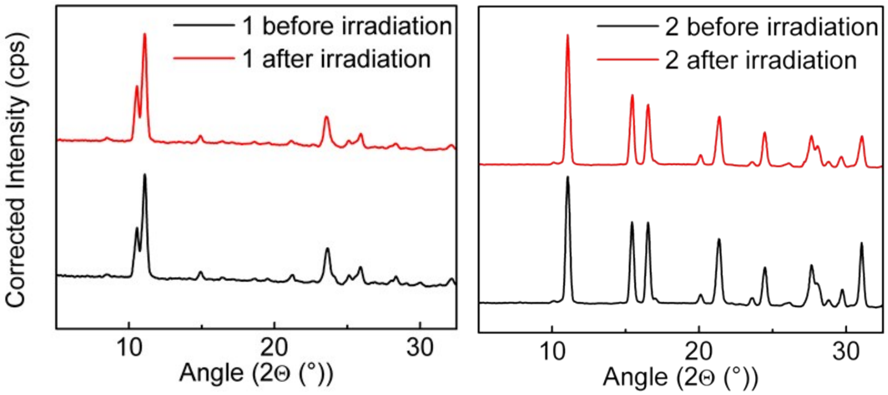

Figure S10. Experimental powder XRD patterns before (black) and after irradiation with high power laser (red) for **CP1** (left) and **CP2** (right).

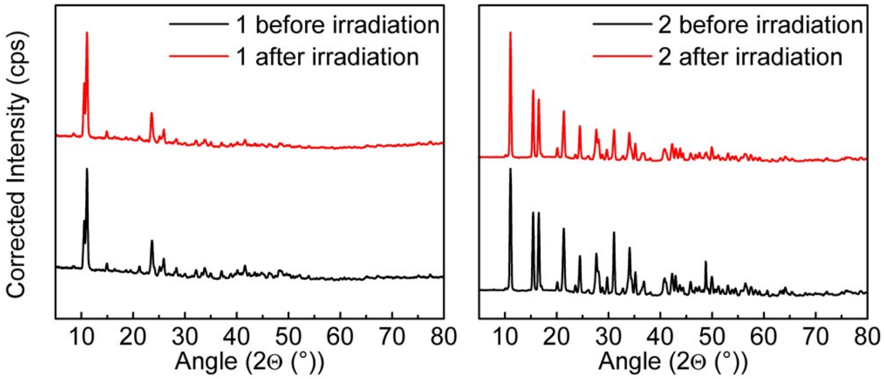

Figure S11: Experimental powder XRD patterns before (black) and after irradiation with high power laser (red) for **CP1** (left) and **CP2** (right).

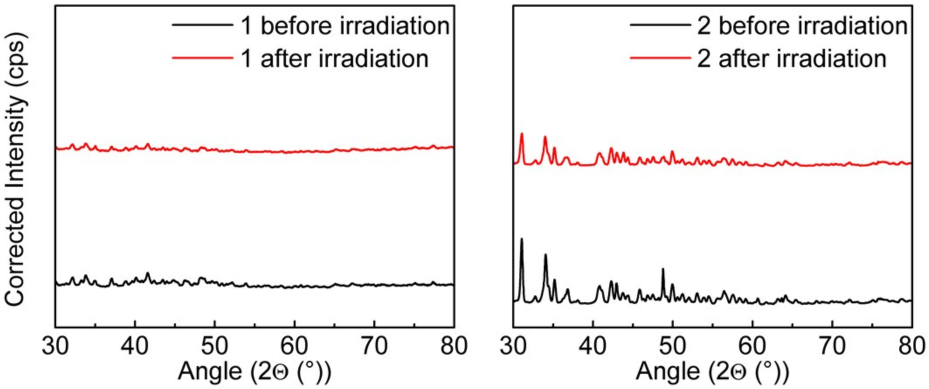

Figure S12: Experimental powder XRD patterns before (black) and after irradiation with high power laser (red) for **CP1** (left) and **CP2** (right) in the large angle region.

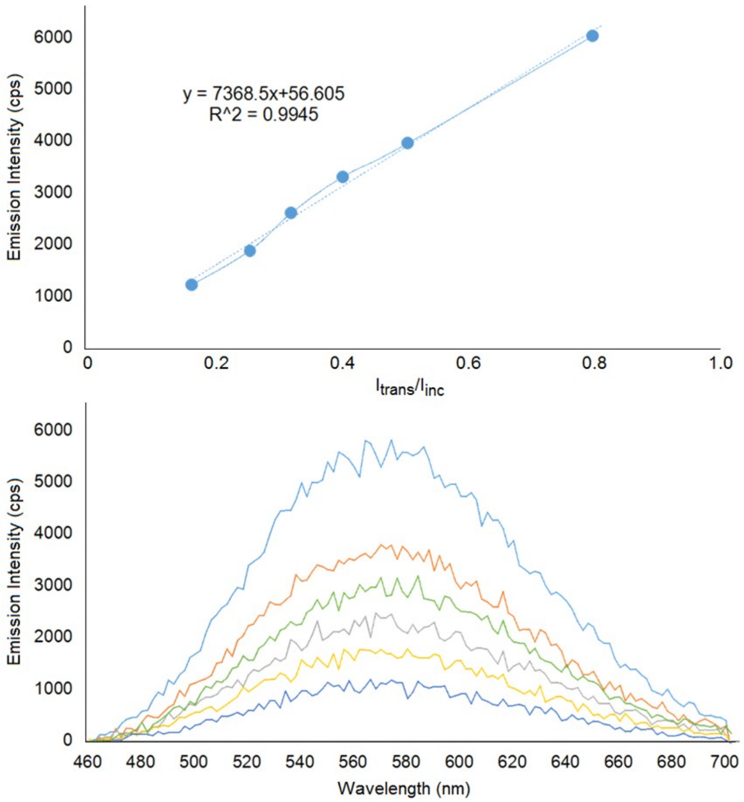

Figure S13. Top: graph reporting the emission intensity of **CP1** *vs* transmitted laser intensity / incident laser intensity at 298 K. The equation is the linear regression illustrated by the dotted line. Bottom: evolution of the emission spectra of **CP1** at 298 K as a function of the same transmitted laser intensity / incident laser intensity ratios in the graph above. The emission spectra are not corrected for the gratings and optics.

TOC

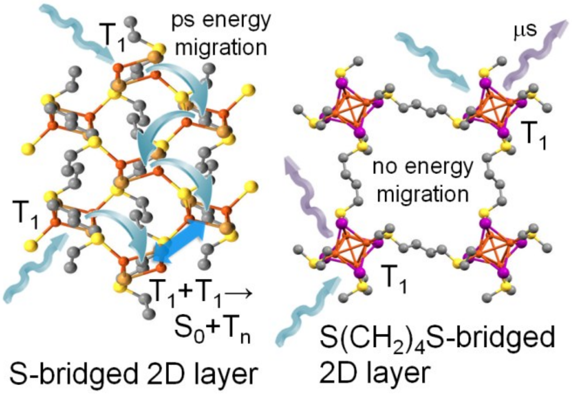
T_1
ps energy migration
μs
T_1
no energy migration
T_1
T_1
$T_1+T_1 \rightarrow S_0+T_n$
S-bridged 2D layer
$S(CH_2)_4S$-bridged 2D layer